Chemical Science

ROYAL SOCIETY OF CHEMISTRY

EDGE ARTICLE

View Article Online
View Journal | View Issue

Cite this: *Chem. Sci.*, 2024, **15**, 20582

All publication charges for this article have been paid for by the Royal Society of Chemistry

Received 1st July 2024
Accepted 12th November 2024

DOI: 10.1039/d4sc04345f

rsc.li/chemical-science

Reactivity of metal hydrides with CO_2: going beyond formate with a high-valent cationic pentahydride Mo(VI) complex†

Nicolas Queyriaux, *[a] Jorge J. Cabrera-Trujillo, [b] Nina Durvin,[a] Laure Vendier,[a] Karinne Miqueu *[b] and Antoine Simonneau *[a]

The cationic molybdenum pentahydride complex $[MoH_5(depe)_2]^+$ (depe = 1,2-bis(diethylphosphino) ethane) is shown to undergo two consecutive reactions with carbon dioxide. In the initial, room-temperature process, classical insertion of CO_2 into a metal–hydride bond is observed, resulting in the formation of the expected formate complex, $[MoH_2(HCOO)(depe)_2]^+$. Further reactivity is triggered at temperature above 100 °C. Complete conversion into two new complexes is indeed observed, resulting from the formal cleavage of a C–O bond of carbon dioxide, $[MoH(CO)_2(depe)_2]^+$ and $[MoO(HCOO)(depe)_2]^+$. Unprecedented in the absence of ligand assistance, such metal hydride reactivity has been comprehensively studied by a combination of experimental and computational means with the aim of elucidating the underlying mechanism that governs this process.

Introduction

Carbon dioxide (CO_2) is an appealing primary source of carbon atoms for the development of new sustainable synthetic procedures of both carbon-based commodity chemicals and fuels.[1–6] Although inexpensive, relatively abundant and non-toxic, CO_2 suffers from severe thermodynamic and kinetic limitations that significantly restrict its use as a routine reagent. Transition metal-based complexes have commonly been employed to overcome this inherent kinetic reluctance.[7–9] They have been demonstrated to be highly effective catalysts for the conversion of CO_2 into a range of hydrogenated C_1 products (HCOOH, CH_3OH and CH_4), either through electro-assisted approaches or *via* traditional catalytic hydrogenation. In the majority of such processes, the formation of a metal formate species through CO_2 insertion into metal hydride bonds represents a fundamental step in catalytic cycles.[10] Consequently, a substantial focus has been directed toward elucidating thermodynamic[11–13] and kinetic[14–18] aspects of this reaction.

Although rare, alternative reactivities of metal hydrides have also been reported (Fig. 1). The group of Parkin described C–O bond cleavage upon exposure of $[Cp^*Mo(PMe_3)_3H]$ to a CO_2 atmosphere, resulting in the formation of a carbonyl complex together with trimethyl phosphine oxide.[19] In the same vein, the group of Milstein investigated the reductive cleavage of CO_2 by hydride complexes of group 9 metals (Rh, Ir) supported by PNP pincer ligands.[20,21] This reactivity, triggered by metal–ligand cooperation, again gave access to carbonyl derivatives – the second oxygen atom being released as a water molecule.

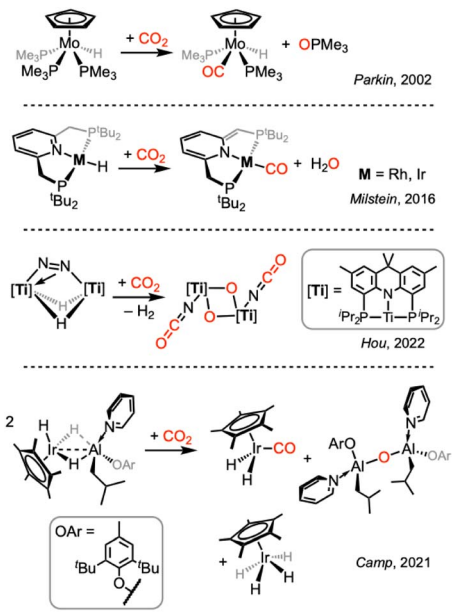

Fig. 1 Examples of C–O bond cleavages in the CO_2 molecule mediated by transition metal hydride complexes.

[a]*LCC-CNRS, Université de Toulouse, CNRS, UPS, 205 Route de Narbonne, BP44099, F-31077 Toulouse Cedex 4, France. E-mail: antoine.simonneau@lcc-toulouse.fr; nicolas.queyriaux@lcc-toulouse.fr*

[b]*CNRS/UPPA, IPREM UMR 5254, E2S-UPPA, Hélioparc, 2 Avenue du Président Angot, 64053 Pau Cedex 09, France. E-mail: karinne.miqueu@univ-pau.fr*

† Electronic supplementary information (ESI) available: Detailed experimental procedures, computational details, NMR and FTIR spectra and crystallographic data. CCDC 2365476–2365478 and 2365557. For ESI and crystallographic data in CIF or other electronic format see DOI: https://doi.org/10.1039/d4sc04345f

Interestingly, a diisocyanato/dioxo dititanium complex was obtained from the stepwise, double reductive cleavage of CO_2 by a dihydride dititanium complex, through the concomitant activation of a dinitrogen ligand.[22] On-metal C–O bond activation by metal hydride complexes can also be facilitated by the assistance of exogenous main-group Lewis acids (LA).[23] Ultimately, such assistance is capable to promote a cooperative reductive cleavage of CO_2, as recently reported by the group of Camp with a strongly polarized heterobimetallic Ir–Al complex.[24] In most of those cases, the transfer of an oxo group to a particularly oxophilic exogenous – or remote – partner thus appears to be an important thermodynamic lever that drives the C–O cleavage reaction.

Recently, our group reported on the isolation of a cationic molybdenum(VI) pentahydride complex supported with a bis(phosphine) ligand,[25] $[MoH_5(depe)_2]^+$ ($\mathbf{1}^+$, depe = 1,2-bis(-diethylphosphino)ethane). Related group 6 pentahydride derivatives were previously postulated, observed or isolated by the groups of Wilkinson,[26] Semenenko,[27,28] Ito,[29] Henderson,[30] Cundari/Yousufuddin[31] and Chirik.[32] Their reactivity towards carbon dioxide remains, however, largely uncharted. In this article, we explore the stoichiometric reactivity of pentahydride complex $\mathbf{1}^+$ towards CO_2 and its nitrogen- and sulphur-based analogues (*N*,*N*′-diisopropylcarbodiimide – DIC – and CS_2). We demonstrate that complex $\mathbf{1}^+$ readily loses H_2 in those processes to generate unsaturated derivatives capable of quick reaction with the considered heterocumulenes. In all cases, insertion of the substrates into a metal-hydride bond occurs. Interestingly, further reactivity is observed for CO_2 upon thermal activation. A rare example of unassisted, on-metal C–O bond cleavage is evidenced, with the formation of both Mo(II)–carbonyl and Mo(IV)–oxo cationic complexes. Comprehensive computational investigations have been conducted to assess the overall mechanism of this intriguing process.

Results and discussion

We have recently reported the protonation behaviour of the neutral Mo(IV) tetrahydride complex **2** towards a variety of proton sources, highlighting the importance of the nature of the conjugate base of the acid used to warrant protonation-only processes.[25] Based on these previous findings, we selected triethylammonium tetraphenylborate $[HNEt_3][BPh_4]$ – that combines both weakly coordinating counter-anion and conjugate base – to serve as the proton purveyor.

Treating a solution of **2** with 1 equiv. of $[HNEt_3][BPh_4]$ at room temperature resulted in the immediate formation of the expected pentahydride complex $[MoH_5(depe)_2][BPh_4]$, $\mathbf{1\cdot BPh_4}$ (Scheme 1). A diagnostic signal appears as a quintet at −5.0 ppm in the hydride region of the ^{1}H NMR spectrum. This complex can be isolated in good yields (80–90%) as a pale-yellow powder.

Single crystals suitable for X-ray diffraction analysis were obtained upon low temperature storage (−40 °C) of THF–pentane solution of the complex. The resulting structure is almost identical to the one we previously reported, should the nature of the counterion be excluded (see ESI†).[25]

When a solution of $\mathbf{1\cdot BPh_4}$ in THF was exposed to CO_2 (3 bar) at room temperature, the solution rapidly turned red. The newly formed complex $\mathbf{3\cdot BPh_4}$ shows a new signal in the hydride region of the ^{1}H NMR spectrum (in $C_6D_4Cl_2$), emerging as a pseudo-quintet at −7.94 ppm with an apparent $^2J_{(P-H)}$ coupling of 42.0 Hz. Another notable, new resonance is observed at 7.77 ppm in the form of a singlet that splits into a doublet ($^1J_{(C-H)}$ = 209.3 Hz) when ^{13}C-labelled CO_2 was used. We assigned this new signal to a formato ligand generated by CO_2 insertion into a Mo–H bond of $\mathbf{1\cdot BPh_4}$. This NMR data is in good agreement with previously reported formato ligands.[33–37] This was further supported by the appearance of a quintet ($^3J_{(C-P)}$ = 3.5 Hz) at 176.1 ppm in the ^{13}C{^{1}H} NMR spectrum of $\mathbf{3\cdot BPh_4}$. The ^{31}P{^{1}H} NMR spectrum features two singlets at 43.9 and 78.3 ppm that expanded into triplets ($^2J_{(P-H)}$ = 36.0 and 41.9 Hz, respectively) upon selective ^{1}H-decoupling centred at 1.5 ppm. Collectively, these results point towards the formulation of $\mathbf{3\cdot BPh_4}$ as $[MoH_2(HCOO\text{-}\kappa^2O)(depe)_2][BPh_4]$ (Scheme 2).[38]

This ion pair crystallised from a THF–pentane solution, and the single-crystal X-ray diffraction (sc-XRD) analysis confirmed the κ^2O bidentate coordination of the formate anion, with Mo–O bond lengths of *ca.* 2.26 Å (Fig. 4). If we restrict to the first coordination sphere, the Mo centre is found in a C_{2v}-symmetric environment. The phosphorus nuclei lie in twos above or under the symmetry plane, in good agreement with the ^{31}P{^{1}H} NMR spectrum showing two resonances. Although the hydrido ligands could not be unambiguously located in the final Fourier difference map, their most likely positions can be estimated from the presence of a large open site located below a mean plane formed by the phosphorus atoms, *trans* to the formato ligand. It is reasonable to propose that the two hydrides should be staggered relative to the formato ligand, so that d orbital destabilization is minimized in an overall dodecahedral geometry, common for 8-coordination.[39]

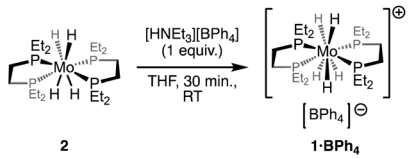

2 **1·BPh4**

Scheme 1 Protonation of **2** employing $[HNEt_3][BPh_4]$ as the proton source affords $\mathbf{1\cdot BPh_4}$.

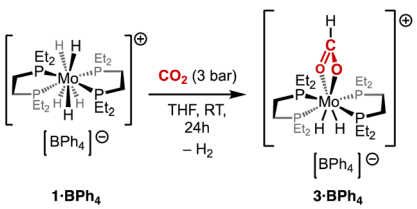

1·BPh4 **3·BPh4**

Scheme 2 Formation of Mo(IV)–formato complex $\mathbf{3\cdot BPh_4}$ from $\mathbf{1\cdot BPh_4}$ under CO_2 atmosphere.

To gain more insight into the reactivity of complex $\mathbf{1}^+$ toward CO_2, we carried out Density Functional Theory (DFT) calculations. We initially performed geometry optimizations at B3LYP-D3(BJ)/SDD+f(Mo), 6-31G** (other atoms) level of theory. Further energy refinement through single point calculations was carried out at PCM(THF)-M06-L-D3/def2-TZVPP level of theory considering solvent effects by means of the Polarizable Continuum Model (PCM) method (see ESI†). Optimization of $\mathbf{3}^+$ was first performed in order to validate the reliability of our selected computational level of theory. We found an excellent agreement between the X-ray and DFT geometries, with a relative error between experimental and calculated structures consistently below 1.5% (Table S1†). We then turned our attention to the mechanistic pathway followed by the reaction of $\mathbf{1}^+$ with CO_2. As illustrated in the reaction profile (Fig. 2), a reductive elimination of H_2 was found to initiate the overall process with a low energy transition state (**TS1**, $\Delta G^{\#} = 4.0$ kcal mol^{-1}) yielding the σ-complex **INT1**. This is followed by a barrierless dissociation of H_2 to afford **INT1′** (Fig. S1†). Further κO^1 coordination of CO_2 to the metal centre then occurs through **TS2** ($\Delta G^{\#} = 22.0$ kcal mol^{-1}). Formation of the resulting **INT2** is slightly endergonic from **INT1′** ($\Delta G = 5.5$ kcal mol^{-1}). Interestingly, kinetic measurements performed under two different pressures of CO_2 (1.5 *vs.* 3 bar) showed no influence of the latter (see ESI†). This agrees with the computed energy profile where H_2 release is energetically more demanding than CO_2 addition. Then, a rapid hydride transfer from the Mo centre to the coordinated CO_2 was found to occur (**TS3**, $\Delta G^{\#} = 0.9$ kcal mol^{-1} from **INT2**), granting further stabilization. We also considered that the hydride transfer process could occur *via* an outer-sphere mechanism, but the corresponding TS was found to be energetically prohibitive at 44.9 kcal mol^{-1} (Scheme S1†). Interestingly, the resulting intermediate **INT3**, featuring a formato ligand, is nearly isoenergetic with **INT1′**, suggesting that CO_2 insertion-deinsertion processes are easily accessible. Rotation around the C–O bond, allowing the expected $\kappa^2 O$ coordination of the formato ligand, finally affords complex $\mathbf{3}^+$ in a global exergonic process (ΔG: −3.0 kcal mol^{-1}). Overall, this mechanism is in good agreement with the concerted CO_2 insertion pathway, previously reported by Hazari for group 9 and 10 metal hydride complexes.[10]

An *o*-dichlorobenzene solution of the $\mathbf{3}\cdot\mathbf{BPh_4}$ complex was heated at 100 °C for 24 hours under an atmosphere of CO_2, resulting in a complex mixture of compounds. Large, unresolved signals were notably observed in the ^{1}H NMR spectrum, suggesting the formation of a paramagnetic molybdenum species identified as $[Mo(depe)_2Cl_2]$ (see ESI†). Simultaneously, the appearance of new resonances in the aromatic domain is also noted. We tentatively assigned those new signals to the formation of biphenyl (see ESI†), arising from the radical-driven reductive rearrangements of the tetraphenylborate anion.[40,41] Slight chemical shift deviations are, however, noted in comparison with an authentic biphenyl sample, which we attribute to the influence of $[Mo(depe)_2Cl_2]$ paramagnetism. We thus decided to opt for the $HB(C_6F_5)_3^-$ anion, that displays increased redox stability. $\mathbf{3}\cdot\mathbf{HB(C_6F_5)_3}$ could easily be prepared by the reaction of **2** with $[\mathbf{HP^tBu_3}][\mathbf{HB(C_6F_5)_3}]$,[25] followed by room temperature reaction with CO_2. Under similar conditions (reaction time increased to 36 h), $\mathbf{3}\cdot\mathbf{HB(C_6F_5)_3}$ indeed granted access to a much cleaner reactivity. More specifically, two new complexes $\mathbf{4}\cdot\mathbf{HB(C_6F_5)_3}$ and $\mathbf{5}\cdot\mathbf{HB(C_6F_5)_3}$ are formed in an approximate 36 : 64 ratio (Scheme 3, top), together with H_2

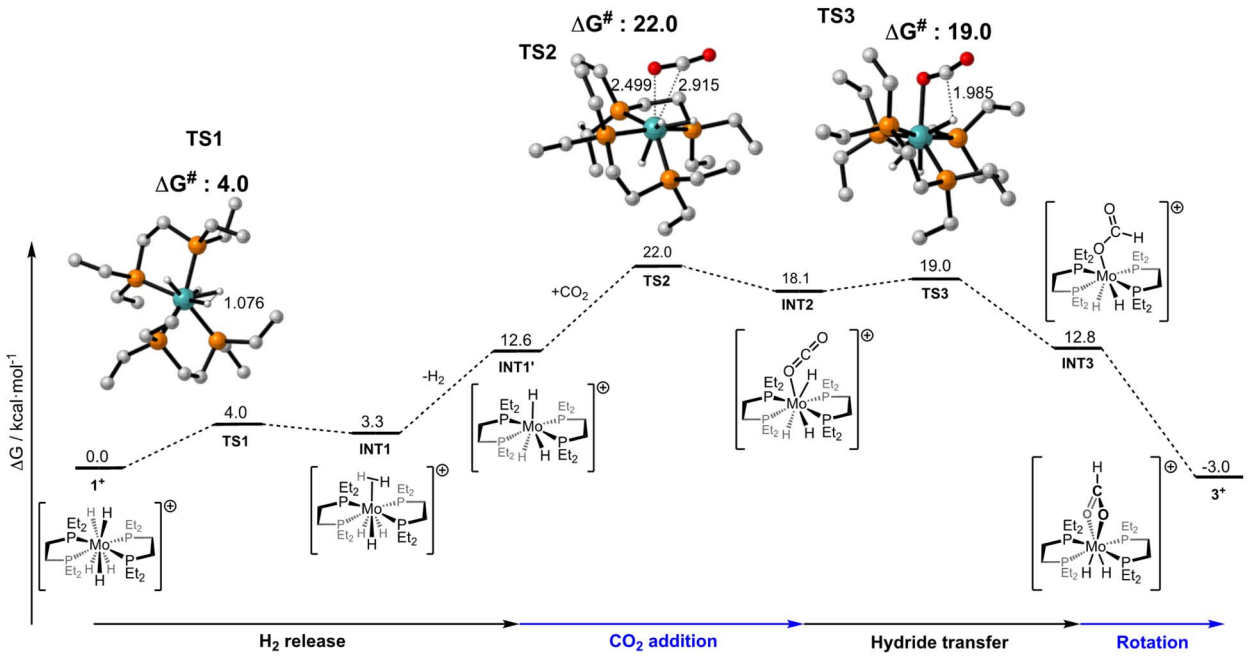

Fig. 2 Computed profile for the reaction of complex $\mathbf{1}^+$ with CO_2. Free energy values (ΔG) and distances are given in kcal mol^{-1} and Å, respectively. All data have been computed at the PCM(THF)-M06-L-D3/def2-TZVPP//B3LYP-D3(BJ)/SDD+f(Mo), 6-31G** (other atoms) level of theory.

evolution. The positively charged part of the minor species was identified as $[MoH(CO)_2(depe)_2]^+$, $\mathbf{4}^+$. This monohydride cationic complex bearing two carbonyl ligands in a *trans* configuration was independently prepared from the reaction of $\mathbf{1}^+$ with CO (Scheme 3, bottom, and Fig. 4). The second complex that formed, $\mathbf{5}^+$, features a singlet at 46.0 ppm in the $^{31}P\{^1H\}$ NMR spectrum. The latter unresolvedly broadens upon selective decoupling of the aliphatic protons, suggesting the absence of hydrido ligands. This is further confirmed by the ^1H NMR spectrum, which is devoid of any new hydride signals. Interestingly, a new proton signal resonating at 7.31 ppm was observed, which correlates with a singlet at 163.8 ppm in the $^{13}C\{^1H\}$ NMR spectrum. This signal splits upon ^{13}C-labeling ($^1J_{(C-H)}$ = 204.3 Hz), indicating the formation of a new formato derivative. High-resolution mass spectrometry was used to gain further insight into the nature of compound $\mathbf{5}^+$. The isotopic pattern of the resulting signal strongly suggests the presence of an additional oxo ligand. Taken together, those results point towards $\mathbf{5}^+$ being formulated as $[MoO(HCOO)(depe)_2]^+$, a cationic Mo(IV) complex. Despite several attempts, independent synthesis of $\mathbf{5}^+$ was unsuccessful: it is, however, interesting to note that ^{31}P NMR features are in line with similar cationic d^2 molybdenum–oxo complexes.[42] Along these two main products, small amounts of free formate was also noticed, accounting for 8% of the non-gaseous compounds ultimately present in solution.

Interested in this unusual process – formally resulting from the cleavage of a CO_2 molecule C–O bond[43] – we again decided to investigate the mechanism of this transformation by the use of DFT calculations. We employed the PCM(*o*-dichlorobenzene)-M06-L-D3/def2-TZVPP//B3LYP-D3(BJ)/SDD+f(Mo), 6-31G** (other atoms) level of theory and corrected the free energies at 373.15 K using GoodVibes package.[44] Two different pathways have been considered for the thermal evolution from complex $\mathbf{3}^+$ to complex $\mathbf{5}^+$. As illustrated in Scheme 4, the first pathway (Pathway I) begins with the reductive elimination of H_2, followed by the coordination of CO_2. Then, the breaking of the C–O bond in the CO_2 ligand occurs, followed by the release of CO leading to the final compound $\mathbf{5}^+$. The second pathway (Pathway II) involves as a first step a hydride transfer from the formato moiety to Mo centre—formally a de-insertion of CO_2, the reverse of the final elementary step in the mechanism leading from $\mathbf{1}^+$ to $\mathbf{3}^+$. H_2 is subsequently released, followed by the C–O bond cleavage in the CO_2 ligand. Finally, two routes were envisaged to achieve the formation of the final product $\mathbf{5}^+$: either CO_2 can be added followed by the release of CO, or CO can be released first, followed by the addition of CO_2. According to our DFT calculations, Pathway I can be safely ruled out due to several high energy barriers in the process (see the complete reaction profile in Fig. S2†). First, the release of H_2 from $\mathbf{3}^+$ is highly endergonic, with the complex **INT4-I** being 25.3 kcal mol^{-1} higher in energy than $\mathbf{3}^+$. Additionally, subsequent addition of CO_2 requires an overall activation barrier of 45.1 kcal mol^{-1}, which cannot be reached under the reaction

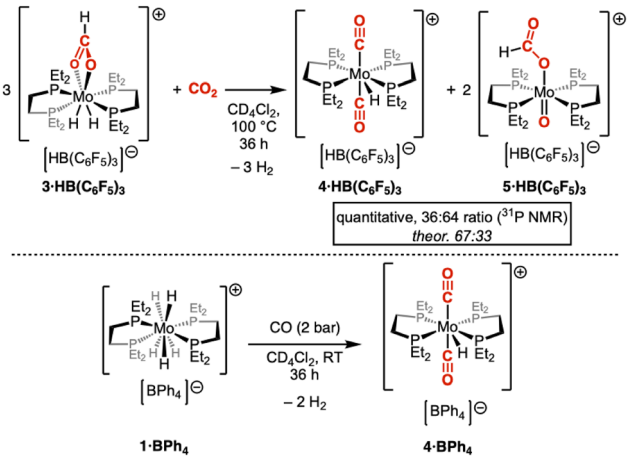

Scheme 3 CO_2 cleavage induced by thermal activation of the formato complex $\mathbf{3}\cdot HB(C_6F_5)_3$ (top) and independent synthesis of the monohydrido bis(carbonyl) complex $\mathbf{4}\cdot BPh_4$ (bottom).

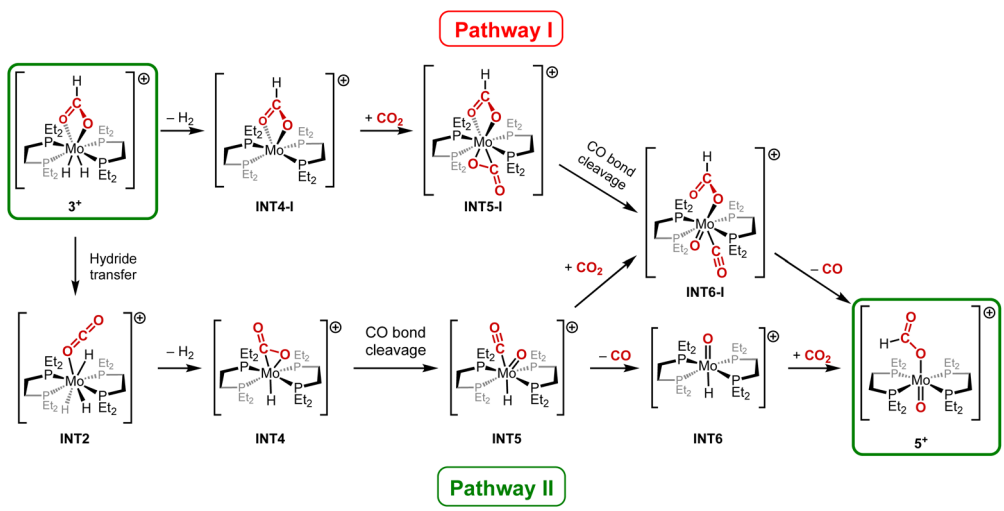

Scheme 4 Plausible reaction pathways for the thermal evolution from $\mathbf{3}^+$ to $\mathbf{5}^+$.

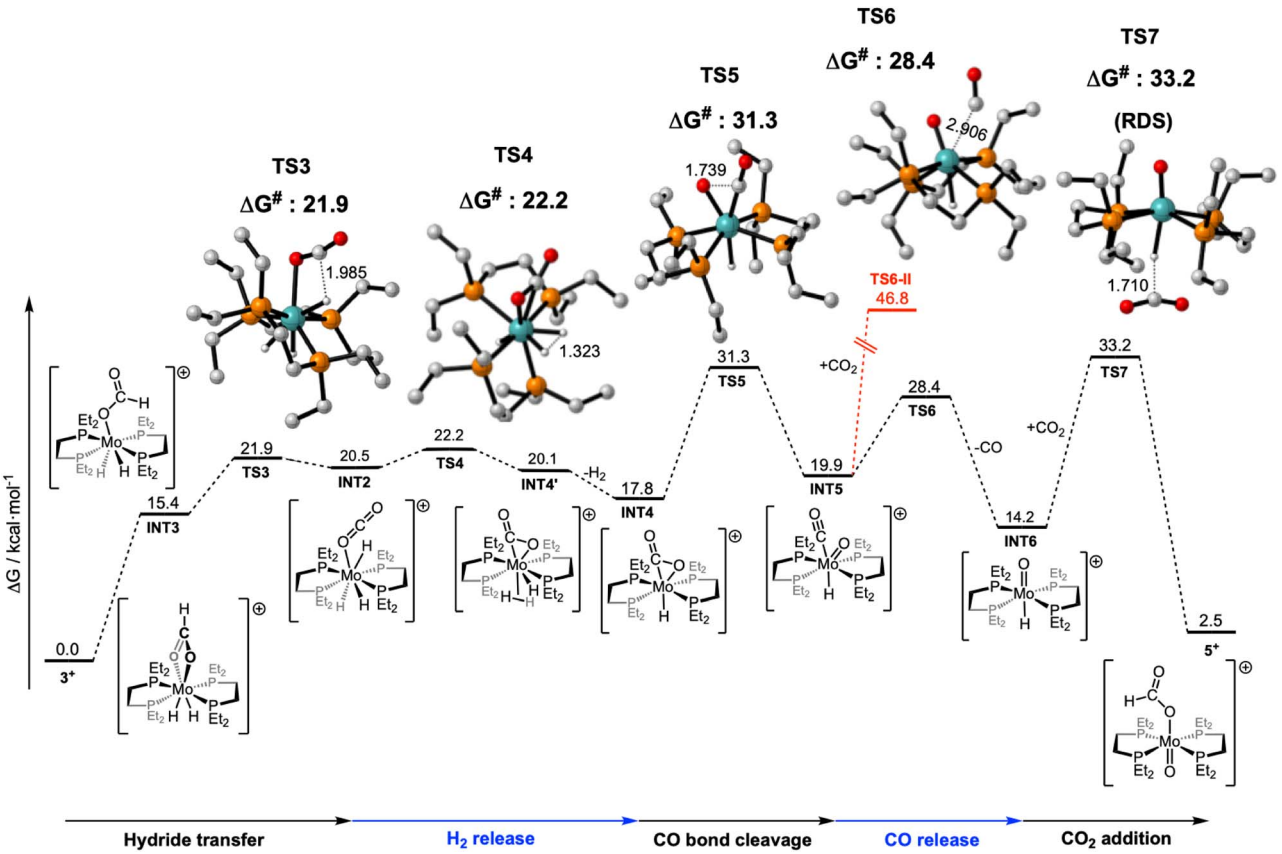

Fig. 3 Energy profile for the thermal evolution of complex 3^+ into complex 5^+ according to Pathway II (Scheme 4). All data have been computed at the PCM(*o*-dichlorobenzene)-M06-L-D3/def2-TZVPP//B3LYP-D3(BJ)/SDD+f(Mo), 6-31G** (other atoms) level of theory. Free energies (ΔG) have been corrected at 373.15 K. All activation barriers are referred to 3^+. Distances and energies are given in Å and kcal mol^{-1}, respectively.

conditions. The transition state for the next step (C–O bond cleavage in the CO_2 molecule) also has a prohibitive high energy at 43.9 kcal mol^{-1}. In the reaction profile corresponding to Pathway II (Fig. 3), the first step formally corresponds to the hydride transfer from the formato moiety to the Mo centre, which is the back-side reaction from 3^+ to **INT2**, previously described in Fig. 2. The reverse activation barrier of 21.9 kcal mol^{-1}, corrected with GoodVibes software to take the temperature into account, was found accessible at 100 °C. Then, the release of H_2 proceeds very easily through **TS4**, with a rather low barrier of 1.7 kcal mol^{-1} from **INT2**, affording the η^2-CO_2–Mo complex **INT4**.[45] The subsequent C–O bond cleavage is energetically more costly, with a transition state, **TS5**, located at 31.3 kcal mol^{-1} above 3^+. Finally, DFT calculations suggest that CO is released (**TS6**) before addition of CO_2 (**TS7**) to form the final product 5^+. In this process, CO_2 plays the role of a hydride abstractor, generating a formato moiety, which finally coordinates on Mo in 5^+. In Pathway II, the rate-determining step (RDS) corresponds to the addition of CO_2 (**TS7**), with an overall activation barrier of 33.2 kcal mol^{-1} from 3^+, which is consistent with a high temperature for the reaction to occur. It is important to note that the released CO (**TS6** in Pathway II) is necessary for the thermal evolution of complex 3^+ into complex 4^+ (Fig. S3†). Additionally, the CO_2 needed for the final step in Pathway II (**TS7**) is derived from the reaction profile described in Fig. S3† (thermal evolution from 3^+ into 4^+). Consequently, formation of 4^+ and 5^+ are intimately connected.

As an extension of our investigation on the activation of CO_2, we studied the reactivity of $\mathbf{1{\cdot}BPh_4}$ with CS_2 and DIC (Scheme 5). Upon treatment of complex $\mathbf{1{\cdot}BPh_4}$ with 1 equiv. of CS_2, an immediate darkening of the THF solution is observed. The formation of complex $\mathbf{6{\cdot}BPh_4}$ was characterized by the appearance of a new quintet at −6.09 ppm ($^2J_{(P-H)} = 44.0$ Hz) and a singlet at 5.76 ppm in the ^{1}H NMR spectrum, as well as a $^{31}P\{^1H\}$ resonance at 69.1 ppm. The latter splits into a doublet ($^2J_{(P-H)} = 44.0$ Hz) upon selective decoupling of the aliphatic protons. Unlike the behaviour observed in the presence of CO_2, these data support a 4e$^-$-reduction of CS_2 through double

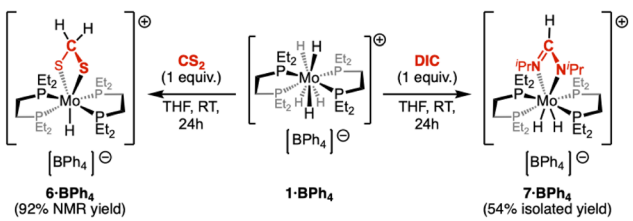

Scheme 5 Formation of $6{\cdot}BPh_4$ and $7{\cdot}BPh_4$ from $1{\cdot}BPh_4$.

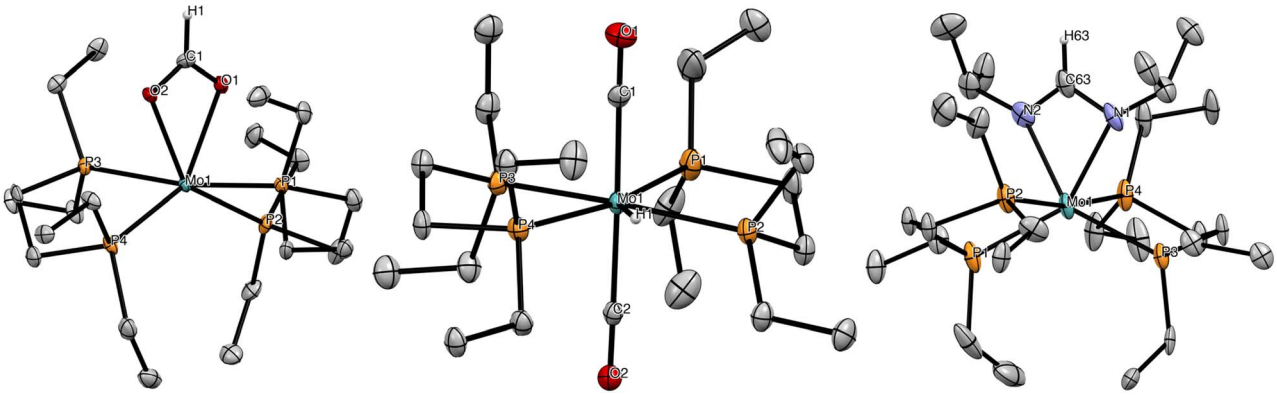

Fig. 4 From left to right, molecular structures of compounds $3\cdot BPh_4$, $4\cdot BPh_4$ and $7\cdot BPh_4$ in the solid state. The BPh_4^- counter ions and the hydrogen atoms (except those on the reduced formato or amidinato ligand or bound to the metal centre) were omitted for clarity. Thermal ellipsoids are shown at the 25% level of probability. Compounds $4\cdot BPh_4$ and $7\cdot BPh_4$ crystallized with two molecules in the asymmetric unit ($Z' = 2$), only one is depicted for clarity.

insertion into Mo–H bonds,[46–49] resulting in a monohydride methanedithiolate derivative, $[MoH(S_2CH_2)(depe)_2][B(C_6H_5)_4]$ ($\mathbf{6\cdot BPh_4}$, Scheme 5). Despite several attempts, $\mathbf{6}^+$ remained reluctant to crystallization and isolation of an analytically pure complex could not be reached (92% spectroscopic purity, see ESI†). Addition of 1 equiv. of DIC to $\mathbf{1\cdot BPh_4}$ in THF led to the formation of the expected M–H insertion product $\mathbf{7\cdot BPh_4}$ (Scheme 5). In the ^{1}H NMR spectrum, loss of the hydride resonance of $\mathbf{1\cdot BPh_4}$ was observed along with the formation of two new diagnostic signals: a multi-lined hydride signal at −7.97 ppm and a singlet at 7.95 ppm assigned to the formamidinate methine proton. Typical of the methine carbon,[50–53] a signal at 159.4 ppm is observed in the $^{13}C\{^1H\}$ NMR spectrum. The $^{31}P\{^1H\}$ features two triplets at 71.0 and 41.5 ppm. Contrary to $\mathbf{6\cdot BPh_4}$, complex $\mathbf{7\cdot BPh_4}$ easily crystallized from a THF–pentane solution, as orange prisms ($\eta = 54\%$). In the solid-state structure of $\mathbf{7\cdot BPh_4}$ (Fig. 4), the formamidinate ligand is found in a κ^2N coordination, with a N–Mo–N bite angle of 59.0°. As expected, this value and other relevant metrics are very similar to those determined in the molecular structure of $\mathbf{3\cdot BPh_4}$. Again, the exact location of the hydrido ligands could not be determined, although their most probable positions will similarly be found *trans* to the formamidinate ligand to fulfil the expected distorted dodecahedral coordination sphere.

Conclusions

In summary, we have thoroughly investigated the reactivity of a high-valent cationic pentahydride Mo(VI) complex $\mathbf{1\cdot BPh_4}$ towards CO_2 and related heteroallenes (CS_2, DIC). The expected insertion of substrate molecules into Mo–H bonds was typically observed, resulting either in two-electron (CO_2, DIC) or four-electron reduction of the substrate (CS_2). Overall, and despite its high-valent character, complex $\mathbf{1\cdot BPh_4}$ behaves as a potent reductant. Most of those reactivities is triggered by facile hydrogen release, suggesting $\mathbf{1\cdot BPh_4}$ could be better described as a masked Mo(IV) complex. Beyond this expected insertion chemistry, we have been able to evidence a rare example of C–O bond cleavage mediated by a metal hydride complex, that occurs without assistance of a ligand or another proximal reactive centre. Indeed, upon thermal activation, the formato complex $\mathbf{5}^+$ was shown to further evolve quantitatively towards a duet of complexes, namely Mo(II)–carbonyl and Mo(IV)–oxo derivatives. This reaction was particularly scrutinized *via* a combination of experimental and theoretical tools. The intimate mechanism responsible for the formation of both carbonyl and oxo derivatives has been carefully deciphered and the importance of high temperature reversible CO_2 hydrogenation–dehydrogenation process was evidenced. Ultimately, this reversibility – together with the high thermodynamic drivers associated with Mo–O bond formation and transient CO liberation – allows on-metal C–O bond cleavage to be accessed.

Data availability

The datasets supporting this article have been uploaded as part of the ESI.†

Author contributions

N. Q. and N. D. run the experiments and analysed the data. J. J. C.-T. performed DFT calculations. L. V. recorded single-crystal X-ray diffraction data and solved the structures. K. M. and A. S. obtained funding for the project, managed it and took part in the analysis of the data. N. Q. wrote the first draft of the manuscript. K. M. and J. J. C.-T. analysed the theoretical results and wrote the computational part of the manuscript. The manuscript was then further revised through contributions of all authors.

Conflicts of interest

There are no conflicts to declare.

Acknowledgements

N. Q. and A. S. are indebted to the European Research Council for funding (ERC Starting Grant No. 757501). Mass

Spectrometry Service (N. Martins-Froment) of the Institute of Chemistry of Toulouse-UAR 2599 (Université de Toulouse, CNRS, Toulouse, France – https://www.ict.ups-tlse.fr) is acknowledged for technical assistance with ESI-HRMS experiments. J. J. C.-T. and K. M. would like to thank the Carnot ISI-FoR institute for its support and funding. The "Direction du Numérique" of the Université de Pau et des Pays de l'Adour and the Mésocentre de Calcul Intensif Aquitain (MCIA) are acknowledged for the support of computational facilities. This work was also granted access to the HPC resources of IDRIS under the allocation 2023-AD010800045R2 made by GENCI. All authors thank their respective institution for providing access to facilities.

Notes and references

1 S. De, A. Dokania, A. Ramirez and J. Gascon, *ACS Catal.*, 2020, **10**, 14147–14185.
2 C. Hepburn, E. Adlen, J. Beddington, E. A. Carter, S. Fuss, N. Mac Dowell, J. C. Minx, P. Smith and C. K. Williams, *Nature*, 2019, **575**, 87–97.
3 J. Artz, T. E. Müller, K. Thenert, J. Kleinekorte, R. Meys, A. Sternberg, A. Bardow and W. Leitner, *Chem. Rev.*, 2018, **118**, 434–504.
4 A. Goeppert, M. Czaun, J.-P. Jones, G. K. Surya Prakash and G. A. Olah, *Chem. Soc. Rev.*, 2014, **43**, 7995–8048.
5 E. V. Kondratenko, G. Mul, J. Baltrusaitis, G. O. Larrazábal and J. Pérez-Ramírez, *Energy Environ. Sci.*, 2013, **6**, 3112–3135.
6 A. M. Appel, J. E. Bercaw, A. B. Bocarsly, H. Dobbek, D. L. DuBois, M. Dupuis, J. G. Ferry, E. Fujita, R. Hille, P. J. A. Kenis, C. A. Kerfeld, R. H. Morris, C. H. F. Peden, A. R. Portis, S. W. Ragsdale, T. B. Rauchfuss, J. N. H. Reek, L. C. Seefeldt, R. K. Thauer and G. L. Waldrop, *Chem. Rev.*, 2013, **113**, 6621–6658.
7 H.-Q. Liang, T. Beweries, R. Francke and M. Beller, *Angew. Chem., Int. Ed.*, 2022, **61**, e202200723.
8 N. W. Kinzel, C. Werlé and W. Leitner, *Angew. Chem., Int. Ed.*, 2021, **60**, 11628–11686.
9 A. Tortajada, F. Juliá-Hernández, M. Börjesson, T. Moragas and R. Martin, *Angew. Chem., Int. Ed.*, 2018, **57**, 15948–15982.
10 N. Hazari and J. E. Heimann, *Inorg. Chem.*, 2017, **56**, 13655–13678.
11 K. R. Brereton, N. E. Smith, N. Hazari and A. J. M. Miller, *Chem. Soc. Rev.*, 2020, **49**, 7929–7948.
12 K. M. Waldie, A. L. Ostericher, M. H. Reineke, A. F. Sasayama and C. P. Kubiak, *ACS Catal.*, 2018, **8**, 1313–1324.
13 E. S. Wiedner, M. B. Chambers, C. L. Pitman, R. M. Bullock, A. J. M. Miller and A. M. Appel, *Chem. Rev.*, 2016, **116**, 8655–8692.
14 J. E. Heimann, W. H. Bernskoetter, N. Hazari and J. M. Mayer, *Chem. Sci.*, 2018, **9**, 6629–6638.
15 D. W. Cunningham and J. Y. Yang, *Chem. Commun.*, 2020, **56**, 12965–12968.
16 M. R. Espinosa, M. Z. Ertem, M. Barakat, Q. J. Bruch, A. P. Deziel, M. R. Elsby, F. Hasanayn, N. Hazari, A. J. M. Miller, M. V. Pecoraro, A. M. Smith and N. E. Smith, *J. Am. Chem. Soc.*, 2022, **144**, 17939–17954.
17 M. R. Elsby, M. R. Espinosa, M. Z. Ertem, A. P. Deziel, N. Hazari, A. J. M. Miller, A. H. Paulus and M. V. Pecoraro, *Organometallics*, 2023, **42**, 3005–3012.
18 J. E. Heimann, W. H. Bernskoetter and N. Hazari, *J. Am. Chem. Soc.*, 2019, **141**, 10520–10529.
19 J. H. Shin, D. G. Churchill and G. Parkin, *J. Organomet. Chem.*, 2002, **642**, 9–15.
20 A. Anaby, M. Feller, Y. Ben-David, G. Leitus, Y. Diskin-Posner, L. J. W. Shimon and D. Milstein, *J. Am. Chem. Soc.*, 2016, **138**, 9941–9950.
21 M. Feller, U. Gellrich, A. Anaby, Y. Diskin-Posner and D. Milstein, *J. Am. Chem. Soc.*, 2016, **138**, 6445–6454.
22 Q. Zhuo, J. Yang, Z. Mo, X. Zhou, T. Shima, Y. Luo and Z. Hou, *J. Am. Chem. Soc.*, 2022, **144**, 6972–6980.
23 Y. Jiang, O. Blacque, T. Fox and H. Berke, *J. Am. Chem. Soc.*, 2013, **135**, 7751–7760.
24 L. Escomel, I. Del Rosal, L. Maron, E. Jeanneau, L. Veyre, C. Thieuleux and C. Camp, *J. Am. Chem. Soc.*, 2021, **143**, 4844–4856.
25 N. Queyriaux, N. Durvin, D. Leon, M.-C. Boegli, L. Vendier and A. Simonneau, *Eur. J. Inorg. Chem.*, 2023, e202300426.
26 E. Carmona-Guzman and G. Wilkinson, *J. Chem. Soc., Dalton Trans.*, 1977, 1716–1721.
27 A. P. Borisov, V. D. Makhaev, G. N. Boiko and K. N. Semenenko, *Koord. Khim.*, 1978, **4**, 1274.
28 V. D. Makhaev, A. P. Borisov, G. N. Boiko and K. N. Semenenko, *Koord. Khim.*, 1982, **8**, 963–969.
29 T. Ito, A. Takahashi and S. Tamura, *Bull. Chem. Soc. Jpn.*, 1986, **59**, 3489–3494.
30 R. A. Henderson, *J. Chem. Soc. Chem. Commun.*, 1987, 1670–1672.
31 C. C. Carter, B. R. Allen, D. V. Bui, D. A. Daley, J. M. Goncalves, C. M. Holinej, S. Lira, D. E. Muniz, A. I. Santiago, N. Sukran, T. R. Cundari and M. Yousufuddin, *Inorganica Chim. Acta*, 2020, **508**, 119638.
32 S. Kim, Y. Park, J. Kim, T. P. Pabst and P. J. Chirik, *Nat. Synth.*, 2022, **1**, 297–303.
33 S. Burling, G. Kociok-Köhn, M. F. Mahon, M. K. Whittlesey and J. M. J. Williams, *Organometallics*, 2005, **24**, 5868–5878.
34 M. L. Christ, S. Sabo-Etienne, G. Chung and B. Chaudret, *Inorg. Chem.*, 1994, **33**, 5316–5319.
35 A. Caise, A. E. Crumpton, P. Vasko, J. Hicks, C. McManus, N. H. Rees and S. Aldridge, *Angew. Chem., Int. Ed.*, 2022, **61**, e202114926.
36 Q. Zhu, J. C. Fettinger and P. P. Power, *Dalton Trans.*, 2021, **50**, 12555–12562.
37 S. Bontemps, L. Vendier and S. Sabo-Etienne, *Angew. Chem., Int. Ed.*, 2012, **51**, 1671–1674.
38 For examples of CO_2 insertion into an Mo–H bond, see: (*a*) D. Lyons, G. Wilkinson, M. Thornton-Pett and M. B. Hursthouse, *J. Chem. Soc., Dalton Trans.*, 1984, 695–700; (*b*) L. K. Fong, J. R. Fox and N. J. Cooper, *Organometallics*, 1987, **6**, 223–231; (*c*) T. Ito and T. Matsubara, *J. Chem. Soc., Dalton Trans.*, 1988, 2241–2242; (*d*) M. Minato, D.-Y. Zhou, K. Sumiura, Y. Oshima,

S. Mine, T. Ito, M. Kakeya, K. Hoshino, T. Asaeda, T. Nakada and K. Osakada, *Organometallics*, 2012, **31**, 4941–4949; (*e*) Y. Zhang, B. S. Hanna, A. Dineen, P. G. Williard and W. H. Bernskoetter, *Organometallics*, 2013, **32**, 3969–3979; (*f*) S. Chakraborty, O. Blacque and H. Berke, *Dalton Trans.*, 2015, **44**, 6560–6570; (*g*) Y. Zhang, P. G. Williard and W. H. Bernskoetter, *Organometallics*, 2016, **35**, 860–865; (*h*) J. A. Buss, N. Shida, T. He and T. Agapie, *ACS Catal.*, 2021, **11**, 13294–13302.

39 J. K. Burdett, R. Hoffmann and R. C. Fay, *Inorg. Chem.*, 1978, **17**, 2553–2568.

40 J. J. Eisch, J. H. Shah and M. P. Boleslawski, *J. Organomet. Chem.*, 1994, **464**, 11–21.

41 P. K. Pal, S. Chowdhury, M. G. B. Drew and D. Datta, *New J. Chem.*, 2002, **26**, 367–371.

42 H. B. Vibbert, A. S. Filatov and M. D. Hopkins, *Angew. Chem., Int. Ed.*, 2020, **59**, 10581–10586.

43 For other examples of C–O cleavage of carbon dioxide with Mo complexes see ref. 19 and: (*a*) R. Alvarez, J. L. Atwood, E. Carmona, P. J. Perez, M. L. Poveda and R. D. Rogers, *Inorg. Chem.*, 1991, **30**, 1493–1499; (*b*) B. L. Yonke, J. P. Reeds, P. Y. Zavalij and L. R. Sita, *Angew. Chem., Int. Ed.*, 2011, **50**, 12342–12346; (*c*) J. A. Buss, D. G. VanderVelde and T. Agapie, *J. Am. Chem. Soc.*, 2018, **140**, 10121–10125.

44 G. Luchini, J. V. Alegre-Requena, I. Funes-Ardoiz and R. S. Paton, *F1000Research*, 2020, **9**, 291.

45 For examples of structurally characterized η^2-CO_2–Mo complexes, see ref. 43c and: (*a*) R. Alvarez, E. Carmona, J. M. Marin, M. L. Poveda, E. Gutierrez-Puebla and A. Monge, *J. Am. Chem. Soc.*, 1986, **108**, 2286–2294; (*b*) L. Escomel, Q. Le Dé, M. Benonie, L. Vendier and A. Simonneau, *Chem. Commun.*, 2024, **60**, 13235–13238.

46 J. Okuda, *Z. Für Naturforschung*, 1990, **45**, 753–754.

47 W. D. Jones and A. D. Selmeczy, *Organometallics*, 1992, **11**, 889–893.

48 T. Gandhi, M. Nethaji and B. R. Jagirdar, *Inorg. Chem.*, 2003, **42**, 667–669.

49 Q. X. Dai, H. Seino and Y. Mizobe, *Eur. J. Inorg. Chem.*, 2011, **2011**, 141–149.

50 E. Lu, Y. Chen and X. Leng, *Organometallics*, 2011, **30**, 5433–5441.

51 J. Cheng and Z. Hou, *Chem. Commun.*, 2011, **48**, 814–816.

52 S. Schulz, T. Eisenmann, S. Schmidt, D. Bläser, U. Westphal and R. Boese, *Chem. Commun.*, 2010, **46**, 7226–7228.

53 Y. Yu, A. R. Sadique, J. M. Smith, T. R. Dugan, R. E. Cowley, W. W. Brennessel, C. J. Flaschenriem, E. Bill, T. R. Cundari and P. L. Holland, *J. Am. Chem. Soc.*, 2008, **130**, 6624–6638.